Automated Annotations of Epithelial Cells and Stroma in Hematoxylin-Eosin Stained Whole Slide Images Using Cytokeratin Restaining

Tomáš Brázdil[1], Matej Gallo[1], Rudolf Nenutil[2], Martin Toufar[1], and Petr Holub[*3]

[1]*Faculty of Informatics, Masaryk University*

[2]*Masaryk Memorial Cancer Institute*

[3]*Institute of Computer Science, Masaryk University*

August 14, 2020

Abstract

Diagnostics of solid tumors of epithelial origin—carcinomas—represents very important part of workload in histopathology. Carcinoma consists of malignant epithelial cells arranged in more or less cohesive clusters of very variable size and shape. In between them there is stroma, comprised by fibroblastic cells, variable amount of extracellular matrix, blood vessels and inflammatory cells of different types. Distinguisting stroma

[*] Corresponding author: Assoc. Prof. RNDr. Petr Holub, Ph.D., Institute of Computer Science, Masaryk University, Botanická 68a, 602 00 Brno, Czech Republic. Email: <hopet@ics.muni.cz>

from epithelium has been already demonstrated to bring critical advantage to artificial intelligence (AI) methods developed to detect carcinomas. In this paper we propose a novel automated workflow that enables large-scale guidance of AI methods. The workflow is based on restaining existing formalin-fixed paraffin-embedded (FFPE) material using panoptic hematoxylin-eosin staining followed by immunohistochemistry to visualize cytokeratins—a cytoskeleton components highly specific to epithelial cells. Compared to existing methods, the currently available hematoxylin and eosin (H&E) stained material can be reused and no additional material, such as consecutive slides, is needed. Based on specifics of the particular staining method, we have developed a robust method to align the restained slides and automatically generate the masks denoting cytokeratin-rich regions, using positions of cell nuclei visible in both original and restained slide. The alignment method has been compared to state-of-the-art method for alignment of consecutive slides and shown that despite being simpler, while still providing sufficient accuracy. The paper also demonstrates how the automatically generated masks can be practically used to train modern AI image segmentation based on U-Net, resulting in very reliable detection of the epithelial regions in the original H&E slides.

1 Introduction

Recently, we can see a rapid onset of deep learning applications in pathology. Despite the real potential of artificial intelligence (AI) assisted histopathology is yet to be determined, the research in this area is expanding and promising. The progress in digitization of histological samples, resulting into virtual slides, so called whole slide images (WSIs). Together with the trend to digitize the whole laboratory workflow, this may change substantially the whole profession, especially if some really useful AI assistance could be implemented. Unfortunately, the development of AI algorithms currently requires a large volume of learning and validation data. For supervised learning these are to be created mostly by manual annotation of histological images, requiring a lot of time and effort from qualified pathologist—the commodities which very often are not readily available.

The solid tumors of epithelial origin (carcinomas) represent a vast and very important part of workload in diagnostic histopathology. The carcinoma tissue is a mixed structure. It consists of malignant epithelial cells arranged in more or less cohesive clusters of very different size and shape. In between them there is stroma, comprised by fibroblastic cells, variable amount of extracellular matrix, blood vessels and inflammatory cells of different types. Some of inflammatory cells also intrude into epithelial islands. The manual annotation of carcinoma as a "whole", can be relatively easy and fast. The information including stroma is very important and data created this way may be useful in some AI applications, especially in diagnosis of malignancy as such, tumor typing and prognostication. From the other side, there are potential AI assistance applications, e.g., counting of mitoses, nuclear morphometry or counting of intraepithelial or stromal lymphocytes, requiring a precise delimitation of epithelial islands and stroma inside the carcinoma, resulting into "epithelial mask", representing the actual annotation. Due to complexity of carcinoma structure, the manual creation of precise epithelial mask is practically impossible, if the representative area of tumor is to be covered for substantial number of carcinoma cases. Differentiating epithelial cancer cells from stroma and inflammatory cells has been already recognized as an important problem, to which solutions using staining consecutive slices of tissue have been proposed [1, 2]. Recent paper [3] demonstrated approach to manual annotations supervised by the cytokeratin mask based on restaining the hematoxylin and eosin (H&E) stained slides using a immunohistochemistry visualize cytokeratins – a cytoskeleton components highly specific to epithelial cells.

The idea behind our project is to develop a working procedure, able to create the epithelial mask in H&E stained carcinoma WSI. The method presented in this paper aims at automating the whole process of epithelium/stroma detection, by (a) developing a method for restaining the slides, which can be automated in staining automata for reproducibility reasons, (b) automated method aligning the restained images in spite of shifts and non-linear tissue transformations that may happened as a consequence of the restaining, (c) automated mask generation based on thresholding. As a demonstrator of the use of the method, it has been applied to guide

machine learning to detect epithelium in the H&E stained tissue microarray (TMA) slides. The use of TMA, the compound histological blocks, containing tens of tumor cores, collected from routine bioptical cases should ensure coverage of adequate number of cases, processed under uniform conditions.

2 Material and Methods

2.1 Material

The sections used for sequential staining represented a leftover material from immunohistochemistry quality control procedure, performed in TMAs containing ten cases of breast carcinoma each. The cases included the most frequent histological patterns, starting from dissociated lobular carcinomas, through trabecular and solid to medullary growth. The cores 2 mm in diameter were bored from routine formalin-fixed paraffin-embedded (FFPE) blocks, manually arranged and embedded as a new block. The source material originated from diagnostic cases evaluated at Department of Pathology, MMCI. All patients provided a written consent to use the leftover material for research. The H&E stained WSI used to evaluate the performance of trained network are part of routine case documentation in the tissue collection at MMCI Biobank. They were selected randomly.

2.2 Restaining protocol

The 5 µm thick sections, cut to distilled water were collected on positively charged slides for immunohistochemistry (TOMO, Matsunami Glass IND LTD, Osaka Japan). The routine H&E staining protocol was performed using Leica autostainer XL5000, followed by routine cover glass mounting using Solakryl BMX (Draslovka, Kolín, Czech Republic) medium using Leica CV500 mounting machine. The details are given in Supplementum Section S1. The slides were left for one hour to dry and then scanned using Pannoramic® MIDI (3DHistech, Budapest, Hungary) with objective 20 at resolution 0.172 µm/pixel. The WSI were uncompressed, in PNG in-

side Mirax format. After that the slides were placed into xylene overnight and left the coverslip to drop off. The another day the immunohistochemistry with cocktail of anticytokeratin antibodies was performed in Dako Autostainer Link 48 (Agilent Santa Clara, United States) using standard staining procedure including deparaffinisation and antigen retrieval. The antibody binding was detected with 3,3'-Diaminobenzidine (DAB) and after repeated nuclear counterstaining with hematoxylin, the slides were dehydrated a mounted in a usual way. The details are given in Supplementum Section S1.

2.3 Data set access

The data set is available as raw files stored in Mirax MRXS format[1] compatible with OpenSlide library [4]. The annotations for the evaluation are available as XML files compatible with ASAP.[2] The data set is pseudonymized and access to it can be requested via BBMRI-ERIC European Research Infrastructure, by following it's access policy[3]; the request should be placed via BBMRI-ERIC Negotiator platform[4] to Masaryk Memorial Cancer Institute.

2.4 Automated alignment of cytokeratin mask on H&E slides

The original H&E-stained TMA slides as well as restained TMA are scanned as WSIs using any of the state-of-the-art scanner. No additional visual cues were needed nor assumed by the methods. Automated generation of aligned cytokeratin mask works in the following steps: (1) the H&E and the restained slide are split into individual tissue cores from the TMA (as shown in Figure 1), (2) cores are registered (aligned) using one of the two methods described below, (3) the resulting mask is created using adaptive thresholding with subsequent noise filtering. The registration method developed by us for the step (2) utilizes specific properties of the restaining to achieve robust results: it uses cell nuclei centroids as reference points, which are visible in both H&E and restained tissue thanks to repeated nuclear counterstaining with hematoxylin.

[1] https://openslide.org/formats/mirax/
[2] https://computationalpathologygroup.github.io/ASAP/
[3] https://www.bbmri-eric.eu/services/access-policies
[4] https://negotiator.bbmri-eric.eu/

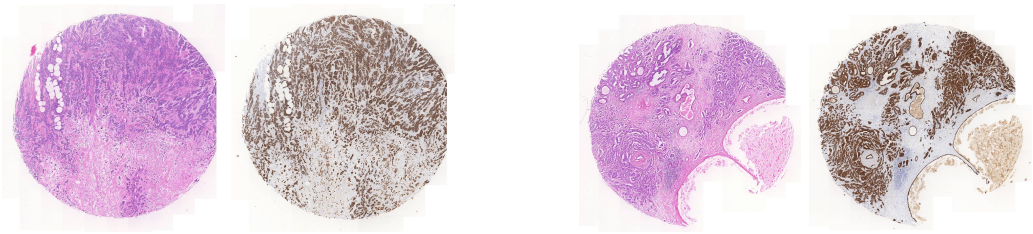

(a) (b) (c) (d)

Figure 1: Pairs of tissue cores extracted from the corresponding TMA scans.

The developed method has been compared to the state-of-the-art registration system designed for alignment of consecutive slides and found more robust.

Nuclei-based registration. We developed a simple yet robust alignment method based on isolation of cell nuclei marked by haematoxylin in both H&E slides as well as restained cytokeratin slides. This method takes the advantage of the cytokeratin restaining protocol introducing the hematoxylin again, thus enabling to identify cell nuclei effectively in both stains. Description of the algorithm refers to the functions defined in Algorithm 1; full pseudocode of the algorithm is available in the Supplementum Section S2.

- The image starts with decomposition of the image into haematoxylin, eosine, and 3,3'-Diaminobenzidine (DAB) channels [5, 6] for both images respectively. For optimization of separation of the 3,3'-Diaminobenzidine (DAB) and haematoxylin channel, the Sparse Non-negative Matrix Factorization (SNMF) method was used [7].

- Cell nuclei centroids are identified in the haematoxylin channel (DETECT-NUCLEI function), taking into account both roundness of the shape and the minimum/maximum size of the nuclei pre-specified for the given resolution.

- The matching of the nuclei centroids in both images is done based searching for minimum square error when doing rigid transformations (TRANSLATION and ROTATION functions) with the gradient descent, and applying $k = 1$ nearest neighbor match.

- Once the best possible match is identified, the pairs of nuclei are used to determine shift vectors for the non-rigid transformation of the image, which is then performed using warp transformation.

```
Function DETECT-NUCLEI(img, numberOfNuclei):
    Segment img using quickshift algorithm, assign each pixel in segment average
      value in segment and separate hematoxylin channel hem;
    for thr in set of evenly spaced numbers over interval (min(hem), max(hem)) do
        Create binary mask of hem with threshold thr;
        Find objects in mask with shape and size of nucleus and compute their
          centroids;
    end
    return set of nuclei centroids, with size larger than numberOfNuclei, created from
      mask with highest threshold, if does not exitst return largest set;
Function ROTATION(sPts, tPts, rotationCenter):
    Generate angles as a set of evenly spaced numbers over interval
      (−minAngle, maxAngle);
    For each angle rotate sPts around rotationCenter and compute average ℓ2 distance to
      nearest-neighbour in tPts;
    return angle where average ℓ2 distance is minimal;
Function TRANSLATION(sPts, tPts, distance):
    Generate set of grids G = {X × X, X is a set of evenly spaced numbers over interval
      (−2^i, 2^i), i ∈ {minDistance, ... , distance}};
    Iterate over grids with decreasing size. For each grid compute all translations, select
      translation where average ℓ2 distance from translated sPts to nearest-neighbour in
      tPts was minimal. Translate sPts with selected translation and add selected
      translation to finalTranslation.;
    return finalTranslation
```

Algorithm 1: Functions used in nuclei-based registration algorithm.

Whole tissue registration. Automatic alignment of consecutive slides using different staining has been tackled by the ANHIR challenge[5] in 2019 [8] and evaluated using landmark validation [9]. This competition did not provide any additional assumptions on the stainings and was based on consecutive slides being restained and not the same slides being restained. Hence the methods had to be more general without being able to use the presumptions on matching

[5] https://anhir.grand-challenge.org/

cell nuclei which we were able to make. One of the top 3 ranking methods, and the only one which has been published as open-source[6] [10], has been used as a basis for comparison of our own method proposed in this paper.

The algorithm combines several methods and proceeds in two stages. First, the initial alignment based on rigid or similarity transformations is computed, then non-rigid transformations finish the registration. For the initial alignment, the system automatically selects between two methods. The first one uses feature detection algorithms (SURF, SIFT, ORB) followed by RANSAC for calculating similarity transformations between features. The second one, related to our algorithm, computes centroids in binary versions of both images (obtained by Li thresholding) and uses them to iteratively compute the desired rotation. For the non-rigid transformation, the system automatically chooses between four methods: local affine transformation with local brightness and contrast corrections, two methods based on Thirion's demons algorithm [11], and a thin plate interpolation applied to all the good matches from the initial alignment procedure.

Automation of cytokeratin mask generation We have tested various methods of thresholding and the isodata method [12, 13] and minimum method [14, 15] provided the best results based on comparison with the pathologists expert knowledge, which is consistent with the surveys of thresholding methods [16–18]. The resulting binary mask has been filtered for objects smaller than fixed threshold (smaller than 60 pixels area in case of our images), which are considered noise.

Due to the different shrinkage of the tissue in the fixation step, shrinkage artifacts often occur; this naturally caused by removing water from the tissue. In our experience, the shrinkage is less for 3,3'-Diaminobenzidine (DAB) restained sample than the original H&E stained sample, because of the immunohistochemistry includes the antigen retrieval step, based on partial hydrolysis of section at high temperature and high pH. This results in the situation where the generated masks are slighly larger than they should be on the H&E staining. Hence we em-

[6] https://github.com/lNefarin/ANHIR_MW

ploy erosion as the last step of the mask generation. However, as discussed in Section 3.1, the whole-tissue-based registration aligns also to tissue edges and thus the shrinkage has been found non-uniform and thus erosion is only applied to nuclei-based registration.

Two representative areas of two different cores have been selected and the border of the epithelium has been carefully marked by experienced pathologist in the H&E staining as a series of precisely placed points – these became *reference points*. The $\ell 2$ distance between the nearest border point of the automatically computed mask from each of the reference points was taken as a metric of alignment. Pairing of the nearest point and the reference point was also inspected visually.

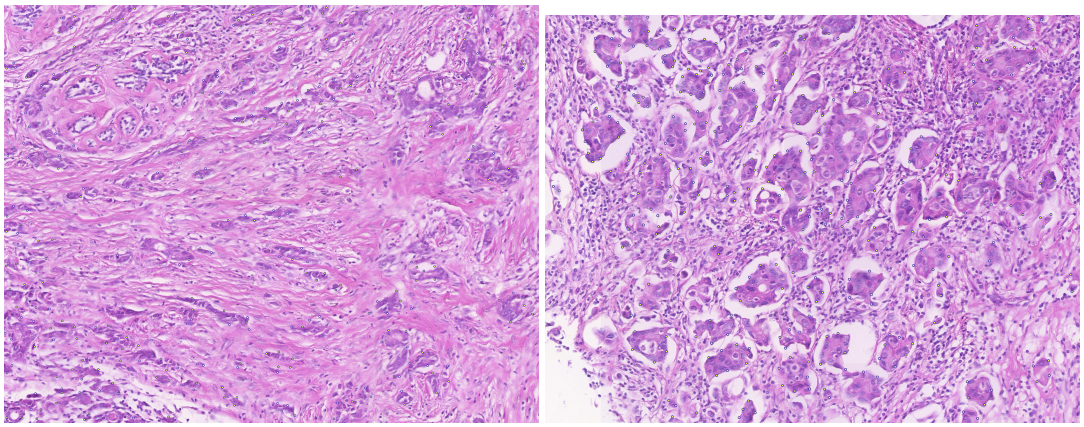

(a) **(b)**

Figure 2: Testing images with reference points. Two different growth patterns of breast carcinoma. Trabecular – dissociated (a) and micropapillary – solid (b).

2.5 Automation of stroma detection in H&E stained tissues

In order to show feasibility and utility of the automated annotation generation, we have developed a simple AI pipeline designed to detect cytokeratin-rich regions in H&E slides.

We used 18 slides to train a classifier: 16 for training, 1 for validation and 1 for testing. Each slide was 6,464 px wide and 6,592 px high. We used the window slide technique with a step size of 128 px to cut the slide into 512 px × 512 px patches. To avoid extraction of patches from background areas of the image we filtered out the background. First we converted the image

from RGB to HSV representation and applied an Otsu's thresholding on the saturation channel of the image. After that we applied closing followed by an opening morphological operation using a disk of size 10.

Before the patches are passed to the network, an image augmentation is applied randomly on each patch. The following augmentations were used: horizontal and vertical flips with 50 % probability each; perturbations to brightness in the range [-64;64]; perturbations to hue and saturation in ranges $[-64;64]$ and $[-10;10]$ respectively. Since there is no canonical orientation for the tissue samples, we can use the flips to artificially increase the training dataset and thus prevent overfitting. The random perturbations serve as a preventative measure against the network relying on a specific colour palette of a slide.

We selected U-Net as our architecture of choice. The minimum number of channels was 64, the maximum was 1,024. The Adam optimizer with binary crossentropy loss function was used to train the network. We initialized the learning rate to 3×10^{-6}. During the training the learning rate was reduced by a factor of 10 after every 4 epochs with no improvement. The network was trained with a batch size of 1 for 30 epochs. In addition to image augmentations, L2 regularization with parameter 1×10^{-3} was used to prevent overfitting.

3 Results and Discussion

We have measured both the accuracy and computational performance of cytokeratin mask generation/registration for both the nuclei-based registration and the whole-tissue-based registration on two selected areas of two distinct cores.

3.1 Generation of masks

Accuracy. We have observed that the cytokeratin mask, extracted by thresholding, typically extends beyond the sample area (as discussed in Section 2.4 and illustrated by Figure 3). Therefore, we have employed standard erosion operation to make the mask smaller so that the proper areas are covered more precisely. We have evaluated the quality of the eroded mask

registration for several sizes of the erosion kernel. The results are presented in Table 1 and more extensive evaluation is provided in Supplementary Tables S3.1 and S3.2; because of non-uniform shrinkage of the mask generated using whole-tissue-based registration, the erosion is only applied to nuclei-based registration and the results for whole-tissue-based registration are provided for reference only in the Supplementum. Note that the table lists only results for small kernels, for larger ones the quality quickly deteriorates.

Erosion [px]	*Mean error [px]*	*Median error [px]*	*MSE*
	Tissue core 2		
0	3.64	3.00	23.37
1	3.50	2.83	20.82
2	3.46	2.83	19.91
3	3.60	3.00	20.90
4	3.88	3.61	23.70
5	4.41	4.00	29.78
	Tissue core 5		
0	5.87	4.24	94.25
1	5.42	4.12	88.03
2	5.10	4.00	83.37
3	4.85	3.61	79.68
4	4.76	3.61	78.39
5	4.85	3.61	79.39

Table 1: Evaluation of mask erosion for nuclei-based registration. Optimum values are 2 px and 4 px for tissue cores 2 and 5 respectively.

The resulting mean error is around 3 px to 6 px. The typical cell size is 15 µm to 20 µm, which in our case roughly corresponds to 80 px to 120 px, and even the size of a nucleus is around 30 px to 40 px. Which means that the error is just a fraction of the size of nuclei. As our goal is to identify groups of epithelial cells, the error is perfectly acceptable.

Note that even though the nuclei-based registration is slightly less precise than the whole-tissue-based registration, the average difference is only around 1 px to 2 px. On the other hand, the nuclei-based registration is straightforward and very easy to understand as opposed to more sophisticated non-linear methods. Hence it is also very consistent and robust. Even when the

tissue is rather damaged during the cytokeratin restaining, the nuclei-based registration works well as long as there is a sufficient amount of nuclei distributed throughout the tissue. On the other hand, the whole-tissue-based registration, truly aligning the tissue borders, might get completely confused as illustrated by Supplementary Figure S3.5.

For a more detailed comparison of the two methods, see the Figure 3. Apparently the whole-tissue-based registration is able to align the mask over the tissue almost perfectly in the case of a well-separated object. The nuclei-based registration is agnostic to the separation of the borders and thus cannot take the advantage of well visible borders. However, once the borders are fuzzy, as in the top part of Figures 3a and 3b, the error of the nuclei-based registration stays consistent as opposed to the whole-tissue-based registration which suddenly distorts the mask in a wrong way.

input : *heImgPts* points on the border of relevant cytokeratin-masked region in H&E stained image, *ctkMask* aligned mask based on cytokeratin
output: μ mean distance from *heImgPts* to closest point on *ctkMask*
1 Let *border* be a set of coordinates where *ctkMask* and eroded *ctkMask* differ;
2 For each point in *heImgPts* find point in *border* with minimal $\ell 2$ distance;
3 **return** mean distance to closest point

Algorithm 2: Algorithm for alignment evaluation.

3.2 Results of H&E Stained Tissue Segmentation

We evaluated the performance of the network in two ways. Firstly, an automated evaluation was performed by calculating the mean intersection over union (IoU) between the predicted mask and the ground truth for every patch. However, the ground truth mask is not perfectly aligned with the original image due to the restaining process used in its creation.

As such we selected 4 additional previously unseen slides. We applied the same preprocessing steps as we did with the original 18 slides and predicted the mask for each patch using the trained network. We then combined all of the patches to reconstruct the full mask. The overlapping regions of the patches were combined using arithmetic mean so the resulting borders

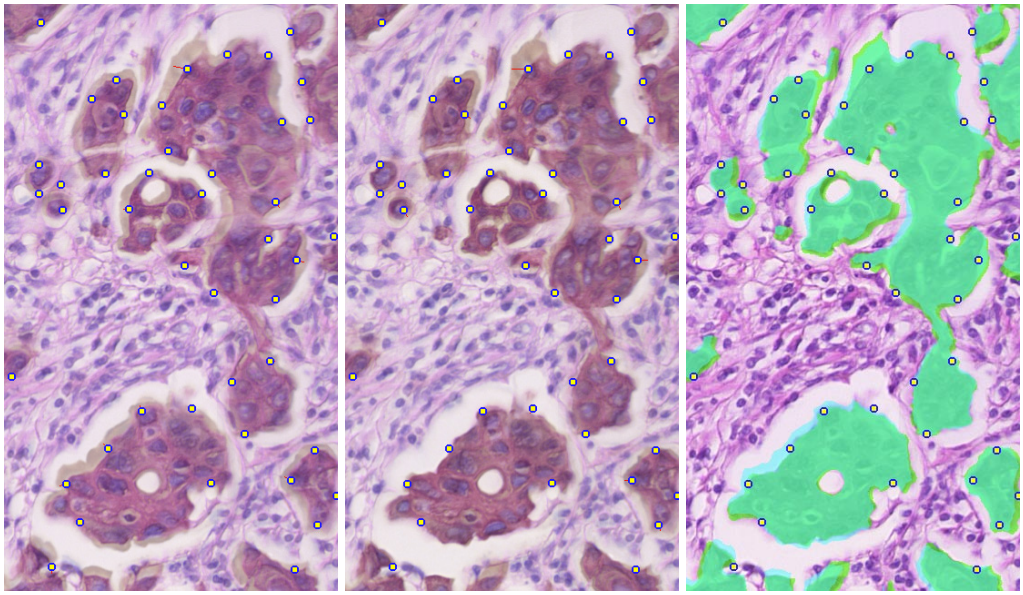

(a) **(b)** **(c)**

Figure 3: Visualization of registrations and masks generated using the two methods discussed in the paper in the crop of Figure 2b. Figures (a) and (b) show orinal H&E stained slide, overlaid with registered slide with cytokeratin visualization using brown 3,3'-Diaminobenzidine (DAB). Red lines are showing distance between each reference point and nearest point on the generated mask. Figure (a) shows the nuclei-based registration; note that the red lines are not touching the brown border of the 3,3'-Diaminobenzidine (DAB) overlay as the final mask is eroded by 3 px as discussed in the method. Figure (b) shows the whole-tissue-based registration. (c) shows difference between the two masks – cyan is generated using nuclei-based registration, green is using whole-tissue-based registration.

are smoother. Lastly a thresholding was applied in which all pixels with combined activation less than 0.5 were zeroed.

We have asked pathologists to manually annotate the four slides. Due to the complexity of the annotation process, the pathologists randomly selected and annotated three sub-regions within each slide while simultaneously avoiding section artifacts. Only these sub-regions have been evaluated and results have been summarized in Table 2. The total average sensitivity across all regions and all slides is 0.81 ± 0.19; and the total average specificity across all regions and all slides is 0.73 ± 0.15.

Table 2: Slide and sub-region evaluation

Slide	Region	Se	Sp	Avg. Se	Avg. Sp
M007	1	0.7535	0.5546	0.7848 ±0.0435	0.7547 ±0.1437
	2	0.8463	0.8858		
	3	0.7544	0.8236		
M025	1	0.8787	0.8537	0.8768 ±0.0186	0.8907 ±0.0308
	2	0.8531	0.9290		
	3	0.8985	0.8893		
M029	1	0.2260	0.6985	0.6638 ±0.3099	0.7193 ±0.0620
	2	0.8651	0.8034		
	3	0.9003	0.6559		
M033	1	0.9324	0.4916	0.9311 ±0.111	0.5596 ±0.0810
	2	0.9169	0.6734		
	3	0.9440	0.5136		

4 Conclusions and Future Work

Detecting carcinomas is one of the focus points of applications of AI methods in digital pathology and guidance of the AI methods by differentiating stroma from epithelium has been demonstrated to significantly improve accuracy. This paper presents a novel method that allows to overcome shortage of whole-slide images manually annotated to differentiate stroma from epithelium. By integrated automated restaining procedure, scanning and image processing pipeline (registration, color channel separation, and thresholding), the whole procedure has potential to generate vast amounts of data suitable for machine learning. Another advantage is that the method can reuse existing H&E stained biological material and hence existing pathology collections can be reused without need for additional biological material. In this paper we have also demonstrated viability of ingesting the resulting pixel-level annotated images into the machine learning pipeline: we trained a U-Net-based image segmentation method to detect epithelium directly in the H&E slides.

As the next step, the method of restaining will be applied to obtain masks from larger set of breast carcinoma TMAs containing about 600 cases. The epithelial areas defined by cytokeratin masks, applied to related H&E scans, will be used to train AI to recognize epithelial areas in

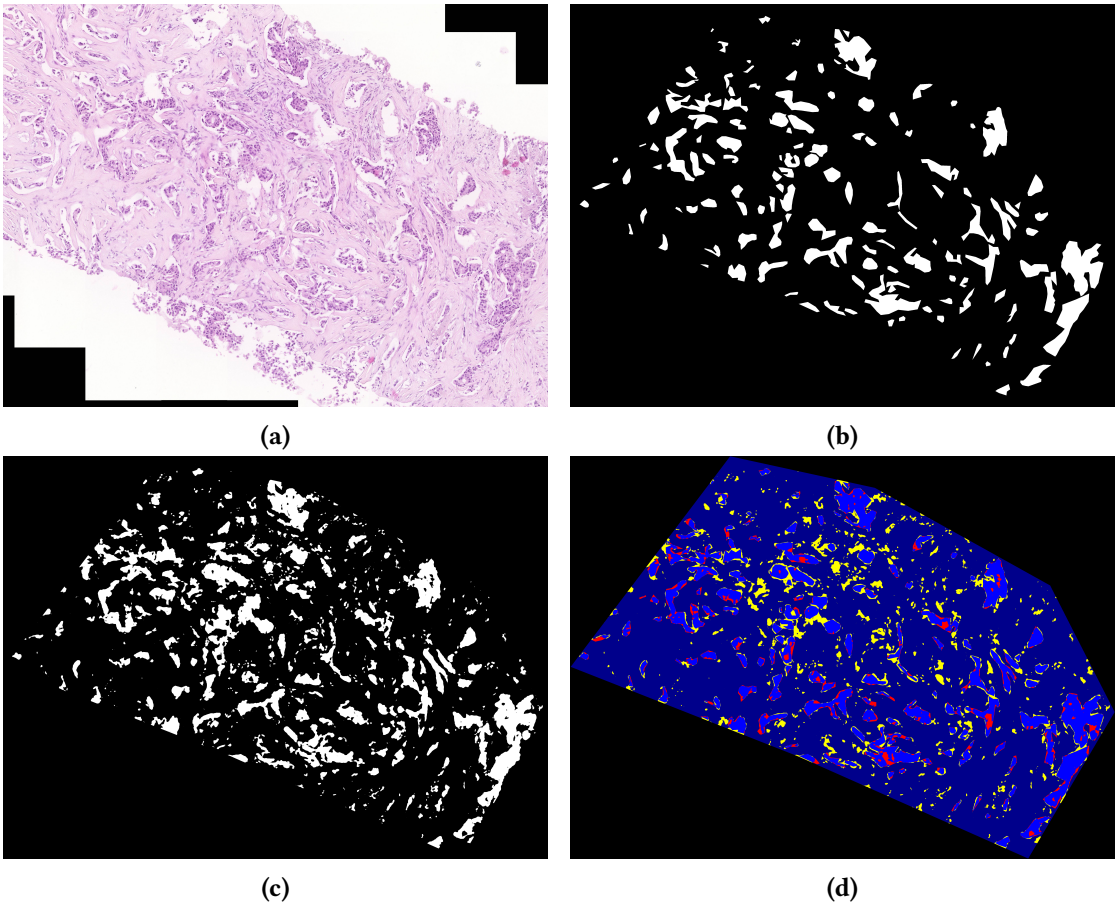

Figure 4: Region 2 from slide M025: (a) H&E region (b) annotations made by a pathologist; (c) predictions made by neural network; (d) heatmap denoting false positives by yellow, false negatives by red, true positives and true negatives by blue

H&E scans more precisely. Once the AI is trained to do this, the sequential staining can be used again in any breast carcinoma sample, but the marker detected by immunohistochemistry can be of researcher‘s choice. In general this can be any marker, where the quantification within different tissue compartments is of potential interest (e.g. Ki67, PD-L1, CD8). Of course, this method can be applied for other diagnoses, e.g., colorectal carcinoma and many more. The more simple potential application is the morphometric analysis in H&E stained sections, e.g., more precise nuclear morphometry, the measurements of epithelial/stromal ratios and epithelial surfaces.

Acknowledgements

This work has been supported by Czech Ministry of Health, (MMCI 00209805) and Czech Ministry of Education, Youth and Sports, (LM2018125).

Author contributions

R.N. selected the material, developed the restaining method and annotated the WSIs. T.B. and P.H. designed and contributed to implementation of the nuclei-based registration method and mask generation method. M.T. contributed to implementation of registration and mask generation methods and performed comparison with the whole-tissue-based registration method. M.G. designed and implemented the AI pipeline to detect epithelium directly in H&E. All co-authors contributed to writing and editing the paper.

Competing interests

Authors declare no competing interests.

References

1. Bengtsson, E. & Ranefall, P. Image Analysis in Digital Pathology: Combining Automated Assessment of Ki67 Staining Quality with Calculation of Ki67 Cell Proliferation Index. *Cytometry Part A* **95,** 714–716. ISSN: 15524930 (2019).
2. Acs, B. *et al.* Ki67 reproducibility using digital image analysis: an inter-platform and inter-operator study. *Laboratory Investigation* **99,** 107–117. ISSN: 15300307 (2019).
3. Valkonen, M. *et al.* Cytokeratin-Supervised Deep Learning for Automatic Recognition of Epithelial Cells in Breast Cancers Stained for ER, PR, and Ki-67. *IEEE Transactions on Medical Imaging* **39,** 534–542. ISSN: 0278-0062 (Feb. 2020).

4. Satyanarayanan, M., Goode, A., Gilbert, B., Harkes, J. & Jukic, D. OpenSlide: A vendor-neutral software foundation for digital pathology. *Journal of Pathology Informatics* **4,** 27. ISSN: 2153-3539 (2013).

5. Ruifrok, A. C. & Johnston, D. A. Quantification of histochemical staining by color deconvolution. *Analytical and Quantitative Cytology and Histology* **23,** 291–299. ISSN: 08846812 (2001).

6. Alsubaie, N., Trahearn, N., Raza, S. E., Snead, D. & Rajpoot, N. M. Stain deconvolution using statistical analysis of multi-resolution stain colour representation. *PLoS ONE* **12,** 1–15. ISSN: 19326203 (2017).

7. Xu, J. *et al.* Sparse Non-negative Matrix Factorization (SNMF) based color unmixing for breast histopathological image analysis. *Computerized Medical Imaging and Graphics* **46,** 20–29. ISSN: 18790771 (2015).

8. Borovec, J., Munoz-Barrutia, A. & Kybic, J. Benchmarking of Image Registration Methods for Differently Stained Histological Slides. *Proceedings - International Conference on Image Processing, ICIP,* 3368–3372. ISSN: 15224880 (2018).

9. Borovec, J. BIRL: Benchmark on Image Registration methods with Landmark validation (2019).

10. Wodzinski, M. & Skalski, A. Automatic Nonrigid Histological Image Registration with Adaptive Multistep Algorithm (2019).

11. Thirion, J. P. Image matching as a diffusion process: an analogy with Maxwell's demons. *Med Image Anal* **2,** 243–260 (Sept. 1998).

12. Ridler, T. & Calvard, S. Picture Thresholding Using an Iterative Selection Method. *IEEE Transactions on Systems, Man, and Cybernetics* **8,** 630–632. ISSN: 0018-9472 (1978).

13. Velasco, F. R. D. Thresholding using the ISODATA Clustering Algorithm. *IEEE Transactions on Systems, Man, and Cybernetics* **10,** 771–774 (1980).

14. Glasbey, C. *An Analysis of Histogram-Based Thresholding Algorithms* 1993.

15. Prewitt, J. M. S. & Mendelsohn, M. L. The analysis of cell images. *Annals of the New York Academy of Sciences* **128,** 1035–1053. ISSN: 00778923 (Dec. 1966).

16. Glasbey, C. A. An analysis of histogram-based thresholding algorithms. *CVGIP: Graphical models and image processing* **55,** 532–537 (1993).

17. Sezgin, M. & Sankur, B. Survey over image thresholding techniques and quantitative performance evaluation. *Journal of Electronic Imaging* **13,** 146. ISSN: 1017-9909 (Jan. 2004).

18. Xue, J. H. & Zhang, Y. J. Ridler and Calvard's, Kittler and Illingworth's and Otsu's methods for image thresholding. *Pattern Recognition Letters* **33,** 793–797. ISSN: 01678655 (2012).